

Stereoscopic Microscopy of Atomic Arrangement by Circularly Polarized-Light Photoelectron Diffraction

H. Daimon

Graduate School of Materials Science, Nara Institute of Science and Technology (NAIST), Ikoma, Nara 630-0101, Japan
(Received 2 August 2000)

A principle for stereoscopic photographs that enables viewing three-dimensional atomic arrangements is proposed. The azimuthal shifts of forward-focusing peaks in the photoelectron diffraction pattern obtained by left and right helicity lights enables a stereoscopic image when the two images are, respectively, viewed by the left eye and the right eye simultaneously. By taking advantage of this phenomenon, a display-type spherical-mirror analyzer can obtain stereoscopic photographs directly on the screen without any computer-aided conversion process.

DOI: 10.1103/PhysRevLett.86.2034

PACS numbers: 61.14.-x, 34.50.Dy

The observation of atomic arrangements, which plays a fundamental role in understanding microscopic phenomena, has been difficult thus far. The scanning tunneling microscope cannot indicate the atomic arrangement because it shows only the corrugation of the surface and not the relation between the top atom and the second layer atoms. Electron microscope images are two-dimensional projections, which cannot show a three-dimensional structure. Usually, LEED (low-energy electron diffraction) or x-ray diffraction analysis is used to obtain detailed atomic positions on a surface. Their analyses are, however, complicated and require many trial-and-error calculations for numerous models.

Recently, many direct methods for three-dimensional analysis have been developed, such as photoelectron holography [1–3], Kikuchi-electron holography [4–6], and fluorescent x-ray holography [7]. Photoelectron holography is powerful because it utilizes the core-level photoelectron diffraction (PD) pattern from a particular atom and produces the atomic arrangement around the specific atom by the Fourier transform of the PD pattern (the hologram). These analyses are direct methods because they do not require a trial model. Although its accuracy is not high (about 0.2 Å), it is useful for the distinction of various models or for making a first trial model for LEED analysis. The problem with these methods is that the data obtained corresponds to reciprocal-space structure, and the real-space structure cannot be imaged before conversion.

In some cases, the PD pattern itself has real-space information of a three-dimensional structure. When the structure is simple, only the measurement of forward-focusing directions is sufficient for three-dimensional analysis [8]. Although the conversion method of this analysis is simple, some processing is also necessary to obtain a three-dimensional structure.

If we can take stereoscopic photographs of an atomic arrangement, our structure recognition would be much improved because we would be able to see the three-dimensional structure directly with our eyes. Here, a new

method to take stereoscopic photographs of atomic arrangements is proposed.

A stereoscopic photograph consists of two different photographs; the left eye focuses on the picture for the left eye, while the right eye focuses on the picture for the right eye at the same time. The positions of an identical object in the two photographs differ by an amount that is almost inversely proportional to the distance from the observer. Assume that you are facing the x direction and looking at object A with your right and left eye at E and F , respectively, as shown in Fig. 1. Both Cartesian coordinates (x, y, z) and polar coordinates (r, θ, ϕ) are used hereafter. When the position of the object A is described as $(R, \theta, 0)$ in polar coordinates, the relation between the distance R and the azimuthal shift $\pm\Delta$ of the object A in the two photographs is described as

$$\Delta = \tan^{-1} \frac{b}{R \sin \theta}, \quad (1)$$

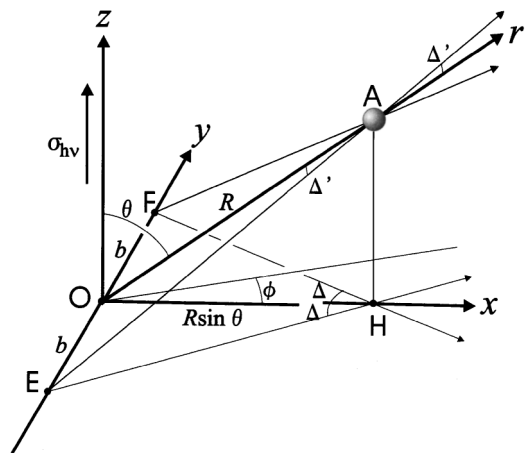


FIG. 1. Relation among various parameters used in the text, such as the distance R , the azimuthal shift Δ of object A simultaneously viewed with the right eye and the left eye (at E and F).

where b is one half of the distance between the two eyes (OE and OF in Fig. 1).

Two photographs of atoms satisfying the condition of Eq. (1) can be obtained by using a display-type spherical-mirror analyzer [9] in the measurement of circularly polarized-light photoelectron diffraction (CPPD). The principle of this method is explained below.

At the kinetic energy of above several hundred eV, the photoelectrons from the emitter atom produce forward-focusing peaks along the direction of surrounding scatterer atoms seen from the emitter [10]. These forward-focusing peaks are the most prominent peaks in the two-dimensional photoelectron diffraction pattern.

For example, the CPPD pattern of W $4f$ photoelectrons from the W(110) surface at a kinetic energy of 800 eV [11] is shown in Figs. 2(a) and 2(b). These patterns were measured by a display-type spherical-mirror analyzer [9] [will be shown in Fig. 4 (below)] which can display the angular distribution of photoelectrons of one particular kinetic energy without distortion. These patterns are observed on a flat screen. The angular range on the screen is about $\pm 60^\circ$. Figures 2(a) and 2(b) were taken with clockwise (cw) and counterclockwise (ccw) circularly polarized light, respectively.

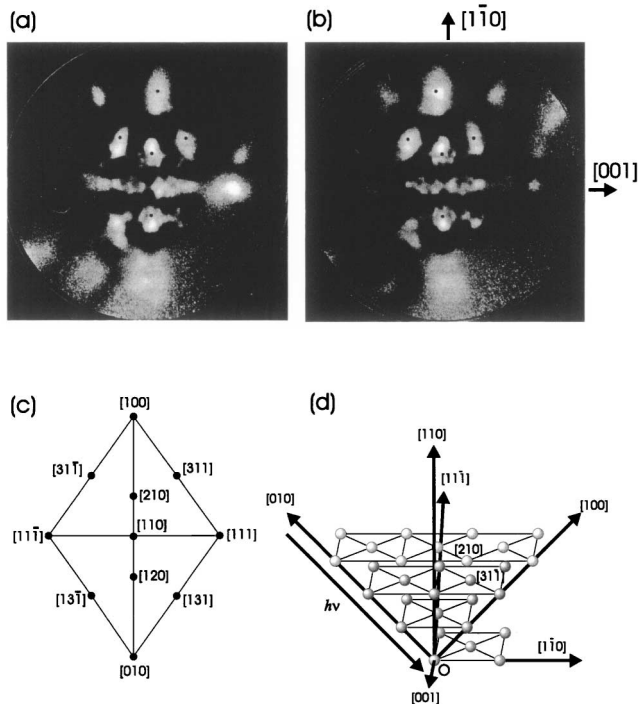


FIG. 2. Two-dimensional circularly polarized-light photoelectron diffraction patterns of W $4f$ from the W(110) surface. (a) and (b) show the results for clockwise and counterclockwise circularly polarized light, respectively. The kinetic energy is 800 eV. The small black circles show the calculated directions of each forward-focusing peak along the crystallographic axes shown in (c). Looking at (a) with the left eye and (b) with the right eye, a three-dimensional arrangement of atoms shown in (d) can be viewed.

The center of the figure corresponds to the surface normal direction, which is the $[110]$ axis, and the vertical direction is $[1\bar{1}0]$. The ccw and cw excitation light is incident 45° inclined to the surface normal, which is the $[010]$ direction, as shown in Fig. 2(d). We can see clear forward peaks around the crystallographic-axis directions such as the $\langle 100 \rangle$, $\langle 111 \rangle$, $\langle 311 \rangle$, and $\langle 210 \rangle$ axes, which are indicated in Fig. 2(c). Although the positions of these forward peaks have been observed along these crystallographic axes in XPD [8], their positions in Figs. 2(a) and 2(b) are slightly different from them. The patterns obtained by cw and ccw light are symmetric with each other with respect to the central vertical line. For example, the $[100]$ peak is slightly off the center to the right in 2(a) and left in 2(b), as shown by dots in the figure.

All these shifts are considered to be a rotation of the forward-focusing peaks with respect to the $[010]$ axis. Such peak “rotations” are of the same qualitative type as seen for Si(001) [12], W(110) 1×1 -O [13], and W(110) 1×1 [11], which was found recently by Daimon *et al.* in the photoelectron diffraction patterns from nonchiral and nonmagnetic systems. The forward-focusing peaks are found to be rotated in the same direction as the direction of rotation of the electric vector of the incident circularly polarized light. This rotation has been explained as being due to the transfer of the angular momentum of photons to the photoelectron, whose z component ratio has been biased while being excited by the circularly polarized light.

The rotation angle Δ of the peak around the photon incident axis is reproduced well by the simple formula [12],

$$\Delta = \tan^{-1} \frac{m}{kR \sin^2 \theta} \cong \frac{m}{kR \sin^2 \theta}. \quad (2)$$

Detailed theoretical works [14–16] also supported this formula. Here, m is the magnetic quantum number (z component angular momentum) of the photoelectron, k is its wave number, R is the internuclear distance between the emitter O and the scatterer A , and θ is the angle between the photon incident direction and the outgoing photoelectron direction. The relation among these directions is also shown in Fig. 1, where the z axis is parallel to the spin of the photon $\sigma_{h\nu}$. When the position vector of the scatterer is described as (R, θ, ϕ) , the peak position observed by using ccw and cw circularly polarized light appears at $(\theta, \phi \pm \Delta)$. If the condition

$$b = m/k \sin \theta \quad (3)$$

is satisfied, this formula (2) is identical to Eq. (1).

Because in both cases [Eqs. (1) and (2)] the angular shift Δ of the object is inversely proportional to the distance R from the emitter, the circularly polarized-light photoelectron diffraction patterns can be considered to be stereoscopic photographs. The necessary condition is that the direction of the photon be parallel to the z axis in stereoscopic photography.

An example is provided in Figs. 2(a) and 2(b). When we look at Fig. 2(a) with the left eye and 2(b) with the right eye, we can view the three-dimensional arrangement of atoms in W(110) crystal. The $\langle 100 \rangle$ (and $\langle 111 \rangle$) atoms look closer, the $\langle 311 \rangle$ and $\langle 210 \rangle$ atoms look farther, and others look the farthest. The $\langle 111 \rangle$ atoms are hardly seen because their peak intensities are much different in Figs. 2(a) and 2(b) due to the imperfection of the tuning of the analyzer. This arrangement almost agrees with the real structure of W(110), as shown in Fig. 2(d). The stereo image is obtained only in the upper half of the pattern. Hence, this stereo view is not perfect here.

The reasons of this imperfection are as follows. The most important reason is that these patterns were measured in an experimental arrangement being not suitable to stereophotography, which will be discussed later. The arrangement used here confines the stereo image to only the upper half. Another reason is that these peaks are not purely composed of the single-scattering forward-focusing peaks but suffer from the interference or multiple scattering originated from nearby peaks, such as $\langle 211 \rangle$ or $\langle 310 \rangle$. Another reason is that the solid angle of these pictures is about $\pm 60^\circ$ in the measurement, whereas it is only $\pm 15^\circ$ when they are viewed by using a stereo viewer.

Here, distortion is defined as the difference of the distance relation in the stereo view of CPPD and that in real structure. We assume here that the forward-focusing peaks are observed at the direction calculated in Eq. (2). When Eqs. (1) and (2) are identical, there is no distortion. The necessary condition is that the right side be constant in Eq. (3). For the objects in the xy plane, there is no distortion because $m/(k \sin\theta)$ is constant. In this case, the magnification ratio is bk/m . When $b = 3$ cm, k is 14 \AA^{-1} (for the kinetic energy of 800 eV), and $m = 4$, the magnification ratio is about 2×10^{10} . When θ is not 90° , the sine function in the denominator of Eq. (3) would make the atoms closer to the viewer as if the distance R had changed to $R \sin\theta$. Hence, the atoms sitting at (R, θ, ϕ) would be seen at $(R \sin\theta, \theta, \phi)$. However, this distortion is hardly present in the actual case because the value m in Eq. (2) is not constant, and its θ dependence is close to $\sin\theta$ when the initial state is other than s core, as discussed in the next paragraph.

Recently, the approximate formula of $m^*(\theta)$, which is the expectation value of m at θ , was derived by Daimon *et al.* [17] as

$$m^*(\theta) = \frac{\sum_{m'=-l'}^{l'} m |c^1(l'+1, m, l', m') \Theta_{l'+1, m}|^2}{\sum_{m'=-l'}^{l'} |c^1(l'+1, m, l', m') \Theta_{l'+1, m}|^2}, \quad (4)$$

where l' is the quantum number of the angular momentum of the initial core state, m' is that of its z component, $l = l' + 1$ and m are those of the final state, $c(lm, l'm')$ is the Gaunt coefficient, and Θ is the polar

angle function of the spherical harmonic $[c^k(lm, l'm') = \sqrt{4\pi/(2k+1)} \iint Y_{lm}^*(\theta, \phi) Y_{k, m-m'}(\theta, \phi) Y_{l'm'}(\theta, \phi) \times \sin\theta d\theta d\phi]$. In this formula, only the final state l of $l' + 1$ was considered and $l = l' - 1$ channel was neglected because the radial matrix element of $l' + 1$ channel is much larger than that of $l' - 1$ channel. The angular dependence of $m^*(\theta)$ of $l = 1, 2, 3$, and 4 final states are shown in Fig. 3. In the above example, the photoelectrons are from the W $4f$ core level, and the outgoing g or $l = 4$ channel is expected to be dominant due to its larger radial matrix element. The black dots in Figs. 2(a) and 2(b) indicate the position calculated using $m^*(\theta)$ for $l = 4$ at each angle. The agreement between the observed and the calculated peak positions is satisfactory.

Figure 3 shows that $m^*(\theta)$ is very close to $\sin\theta$ except for $l = 1$. The $l = 1$ state has a constant value of $m^*(\theta) = 1$ because there is only one final state of $m = 1$. $m^*(\theta)$ for $l = 2$ becomes closer to $\sin\theta$ when $m^*(\theta)$ is calculated more strictly [17]. Hence, the distortion of the stereo view is very small except for $l = 1$.

The distortion of the stereo image from the real structure is calculated for the case of $l = 4$ using $m^*(\theta)$ of Eq. (4). We assumed $b = m^*(90^\circ)/k = 0.22(\text{\AA})$. This quantity b is known as the impact parameter in collision theory, according to which it can be related to the angular momentum through the equation of $m^*(90^\circ)\hbar = \hbar kb$. The analysis shows that the distortion of the viewed image is less than 1% within $\pm 30^\circ$ from the horizontal direction ($60^\circ < \theta < 120^\circ$) and less than several percent in $\pm 60^\circ$. Note that this distortion due to m^* depends only on l , but hardly depends on atomic species or the kinetic energy of photoelectrons.

In the above analysis, we assumed that (i) the forward-focusing peaks are clearly seen in the photoelectron diffraction pattern, and (ii) the positions of the peaks are well reproduced by Eq. (2). These restrictions will determine the range of applicability of this analysis. The first restriction implies that the emitter atom must lie

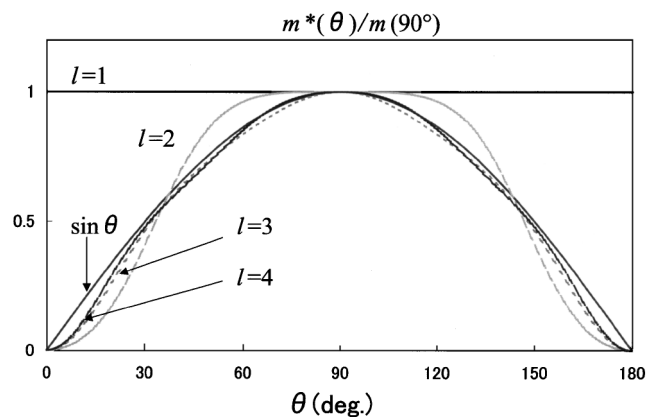


FIG. 3. Angular dependence of the effective m value $m^*(\theta)$ of $l = 1, 2, 3$, and 4, which corresponds to the photoelectrons from initial states of s, p, d , and f core, respectively.

under the scatterer atoms and that the kinetic energy of the photoelectron should be above several hundred eV. In an actual case, photoelectron diffraction and the multiple-scattering effect could modify the forward-focusing peaks, which could complicate the analysis. The peak positions, however, have been reproduced well thus far not only for the adsorbate single-scattering case [13] but also for the bulk multiple-scattering case when the forward-focusing peaks are clearly seen [11]. Hence, this analysis seems to be applicable not only for the molecules adsorbed on surfaces but also approximately for the crystalline substance. A metal-organic complex such as hemoglobin is one of the best candidates of this stereophotography, in which the atomic arrangement around the central metal atom would be seen.

Other possible complications in the practical use may arise for lower-symmetry surfaces such as Si(001). The observed pattern would be a mixture of those from different domains, and the stereo image will be duplicated or triplicated according to the symmetry of the surface.

Using a display-type spherical-mirror analyzer [9], this stereoscopic photograph can be obtained directly on the screen without any computer-aided conversion process. Any two-axis rotatable analyzer capable of measuring photoelectrons two-dimensionally can also take this stereoscopic photograph with the aid of a computer. Notice that a two-dimensional photoelectron data-collection system "with rotating sample" cannot obtain stereoscopic photographs. Other types of display analyzers such as the Eastman-type analyzer can also be used to take stereoscopic photographs. In this case, however, the pattern obtained on the screen is distorted, and computer processing is inevitably necessary to make the photograph. Because the display-type spherical-mirror analyzer can obtain a distortion-free image in much wider solid angles than the Eastman-type one, it is the best analyzer to take the stereoscopic photographs.

When the time required to change the helicity of circularly polarized light is reduced and signal intensity increases, this display analyzer will give an opportunity for real-time stereoscopic observation. In this case, both patterns will be displayed in a stereoscopic manner, such as side by side, alternatively in time, or overlapped with different colors. Real-time observation will help in understanding the dynamics of atoms. Although it takes about 30 min at present to obtain the photograph because the signal intensity is not very high, the development of synchrotron radiation and measurement techniques will continue to shorten the measurement time. In the near future, measurement times at least as short as that of "real-time" video rate will be achieved.

The best arrangement of the apparatus is that the center of the screen corresponds to $\theta = 90^\circ$. This condition is realized when the light is incident perpendicular to the analyzer entrance axis as shown in Fig. 4. In this case, almost distortion-free stereoscopic photographs of $\pm 60^\circ$ ($30^\circ < \theta < 150^\circ$) are displayed on the screen.

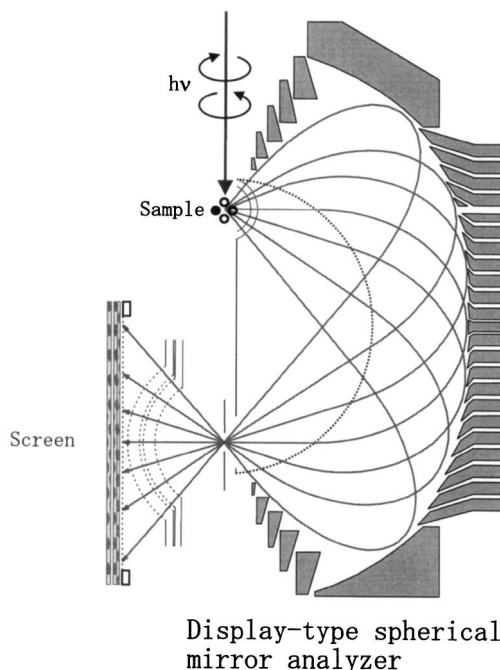


FIG. 4. The best arrangement for stereoscopic photography, in which the circularly polarized light is incident perpendicularly to the two-dimensional analyzer axis.

The author is indebted to Y. Miyatake, K. Enomoto, M. Kotsugi, T. Nakatani, T. Matsushita, K. Hattori, A. Kobayashi, and K. Fukumoto for performing the experiment. This study was supported by a Grant-in-Aid for Specially Promoted Research Projects from the Ministry of Education, Science, Sports, and Culture, Japan.

- [1] A. Szoke, in *Short Wavelength Coherent Radiation: Generation and Applications*, edited by D.T. Attwood and J. Bokor, AIP Conf. Proc. No. 147 (AIP, New York, 1986).
- [2] J.J. Barton, *Phys. Rev. Lett.* **61**, 1356 (1988).
- [3] T. Nakatani *et al.*, *J. Synchrotron. Radiat.* **3**, 239 (1996), and references therein.
- [4] G.R. Harp, D.K. Saldin, and B.P. Tonner, *Phys. Rev. Lett.* **65**, 1012 (1990).
- [5] I.H. Hong *et al.*, *Surf. Rev. Lett.* **4**, 733 (1997), and references therein.
- [6] C.Y. Chang, Y.C. Chou, and C.M. Wei, *Phys. Rev. B* **59**, R10453 (1999).
- [7] C.S. Fadley and P.M. Len, *Nature (London)* **380**, 27 (1996).
- [8] H. Daimon *et al.*, *Surf. Sci.* **408**, 260 (1998).
- [9] H. Daimon, *Rev. Sci. Instrum.* **59**, 545 (1988); **61**, 205(E) (1990).
- [10] C.S. Fadley, in *Synchrotron Radiation Research: Advances in Surface Science* (Plenum, New York, 1990).
- [11] K. Enomoto *et al.*, *Surf. Rev. Lett.* **7**, 643 (2000).
- [12] H. Daimon *et al.*, *Jpn. J. Appl. Phys.* **32**, L1480 (1993).
- [13] H. Daimon *et al.*, *Phys. Rev. B* **58**, 9662 (1998).
- [14] A.P. Kaduwela *et al.*, *Phys. Rev. B* **52**, 14297 (1995).
- [15] P. Rennert *et al.*, *J. Phys. Soc. Jpn.* **66**, 396 (1997).
- [16] A. Chasse and P. Rennert, *Phys. Rev. B* **55**, 4120 (1997).
- [17] H. Daimon *et al.*, *Surf. Sci.* **471**, 143 (2001).